Accuracy of Individual Trabecula Segmentation Based Plate and Rod Finite Element Models in Idealized Trabecular Bone Microstructure

Hong Wang
Department of Engineering Mechanics,
School of Aerospace Engineering,
Tsinghua University,
Beijing 100084, PRC
e-mail: wanghong06@mails.tsinghua.edu.cn

X. Sherry Liu
McKay Orthopaedic Research Laboratory,
University of Pennsylvania,
Philadelphia, PA 19104
e-mail: xiaoweil@mail.med.upenn.edu

Bin Zhou
e-mail: bz2159@columbia.edu

Ji Wang
e-mail: jw2857@columbia.edu

Bone Bioengineering Laboratory,
Department of Biomedical Engineering,
Columbia University,
New York, NY 10027

Baohua Ji
Biomechanics and Biomaterials Laboratory,
School of Aerospace Engineering,
Beijing Institute of Technology,
Beijing 100081, PRC
e-mail: bhji@bit.edu.cn

Yonggang Huang
Department of Civil and Environmental Engineering,
Northwestern University,
Evanston, IL 60208
e-mail: y-huang@northwestern.edu

Keh-Chih Hwang
Department of Engineering Mechanics,
School of Aerospace Engineering,
Tsinghua University,
Beijing 100084, PRC
e-mail: huangkz@mail.tsinghua.edu.cn

X. Edward Guo[1]
Bone Bioengineering Laboratory,
Department of Biomedical Engineering,
Columbia University,
New York, NY 10027
e-mail: ed.guo@columbia.edu

Currently, specimen-specific micro finite element (μFE) analysis based micro computed tomography (μCT) images have become a major computational tool for the assessment of the mechanical properties of human trabecular bone. Despite the fine characterization of the three-dimensional (3D) trabecular microstructure based on high-resolution μCT images, conventional μFE models with each voxel converted to an element are not efficient in predicting the nonlinear failure behavior of bone due to a prohibitive computational cost. Recently, a highly efficient individual trabecula segmentation (ITS)-based plate and rod (PR) modeling technique has been developed by substituting individual plates and rods with shell and beam elements, respectively. In this technical brief, the accuracy of novel PR μFE models was examined in idealized microstructure models over a broad range of trabecular thicknesses. The Young's modulus and yield strength predicted by simplified PR models strongly correlated with those of voxel models at various voxel sizes. The conversion from voxel models to PR models resulted in an ~762-fold reduction in the largest model size and significantly accelerated the nonlinear FE analysis. The excellent predictive power of the PR μFE models, demonstrated in an idealized trabecular microstructure, provided a quantitative mechanical basis for this promising tool for an accurate and efficient assessment of trabecular bone mechanics and fracture risk.
[DOI: 10.1115/1.4023983]

Introduction

Osteoporosis is characterized by low bone mass and microarchitectural deterioration of trabecular bone [1] leading to bone fragility and high fracture risk [2–5]. Based on high resolution micro computed tomography (μCT), micro finite element (μFE) models have been widely utilized to assess trabecular bone mechanical properties and have shown excellent prediction power compared with experimental measurements [6,7]. However, voxel-based μFE models are not efficient in clinical applications because of its prohibitive computational cost. Besides, the micromechanics of trabecular bone is not easily accessible by the cumbersome voxel-based μFE models, since it is difficult to navigate through millions of elements in order to examine individual trabecular failure. Therefore, there is a strong need for an alternative approach that advances in efficiency, while maintaining the fine three-dimensional (3D) architectural details of trabecular bone.

Recently, a novel plate and rod (PR) μFE modeling technique has been developed based on individual trabecula segmentation (ITS), which significantly simplifies trabecular microarchitecture as a combination of individual trabecular plates and rods [8–10]. An ITS-based morphological analysis allows for the separate assessment of trabecular plates and rods regarding volume, orientation, thickness, and connectivity, which has added tremendous insight about the distinct roles of plates and rods in governing the mechanical properties and failure behaviors of trabecular bone [2,11,12]. The ITS measurements of clinically available high resolution peripheral quantitative CT (HR-pQCT) images have furthermore demonstrated its capacity to detect subtle but important microstructural changes in osteoporosis and its treatment [13–15] and to discriminate fracture status independent of areal bone mineral density [16]. Computationally, one can model individual rods/plates by beam/shell elements, respectively. These specimen-specific PR μFE models show great promise in efficiently and accurately predicting the mechanical properties of trabecular bone.

The objective of this technical brief was to examine the accuracy of PR μFE models in predicting Young's moduli and yield strengths of idealize trabecular bone microstructural models, which allows fundamental accuracy testing independent of biological variations and image noise, etc. Human trabecular bone varies greatly in density and microarchitecture across anatomic sites [8]. Trabecular bone microstructure captured by μCT depends on the image resolution and signal-to-noise ratio [14]. A variety of

[1]Corresponding author.

Contributed by the Bioengineering Division of ASME for publication in the Journal of Biomechanical Engineering. Manuscript received September 5, 2012; final manuscript received January 14, 2013; accepted manuscript posted March 16, 2013; published online April 5, 2013. Assoc. Editor: Yener N. Yeni.

trabecular bone mechanical behaviors have been simulated by such idealized models as elastic deformation, fatigue damage accumulation, and trabecular bone loss in osteoporosis [17–22]. In this study, idealized plate-rod and rod-rod microstructures of various thicknesses were constructed at typical resolutions of μCT or HR-pQCT images. Voxel-based and PR μFE models were generated and subjected to FE analysis for predicting Young's moduli and yield strengths.

Methods

Construction of Idealized Microstructure. In an idealized plate-rod microstructural model, two square plates 1000 $\times$ 1000 μm^2 were connected by four 1000 μm-long rods in a unit cell (see Fig. 1(*a*)). An idealized rod-rod model consisted of eight interconnected 1000 μm-long rods in a unit cell (see Fig. 1(*b*)). The thickness of the plates and the diameter of the rods varied in 80, 160, 240, and 320 μm increments. Then, simulated μCT images were constructed for each model at three isotropic voxel sizes: 20, 40 (typical μCT images of human samples), and 80 μm (typical clinical HR-pQCT images). The simulated μCT images were binary matrices representing the 3D trabecular microstructure in the same manner as an actual μCT scan.

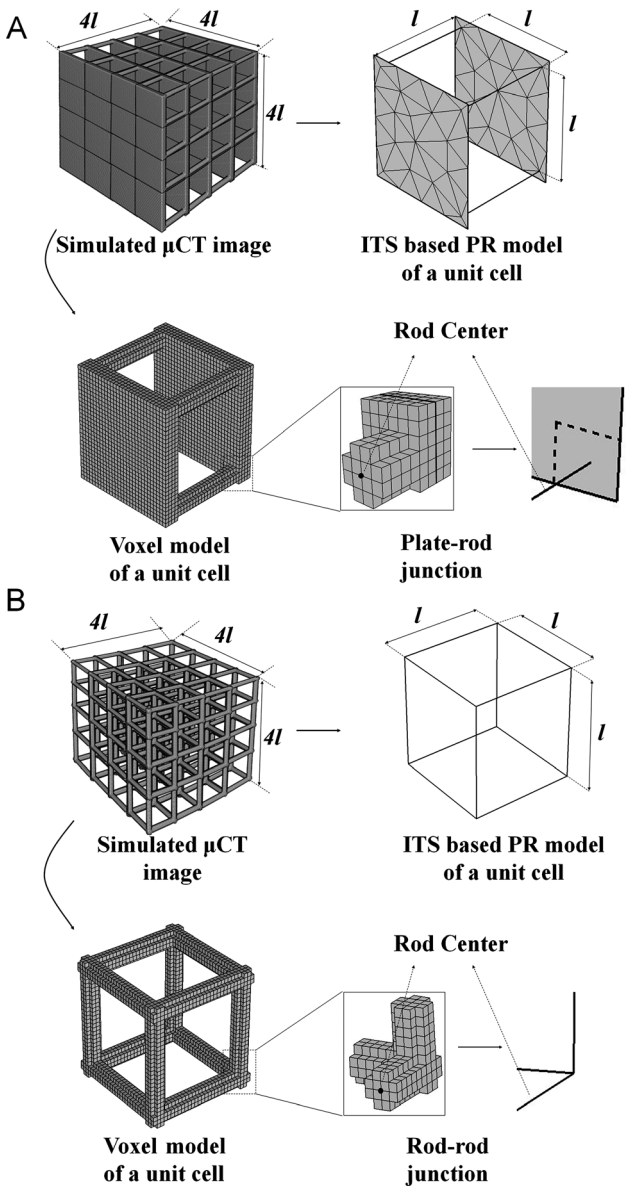

Fig. 1 Schematics of the experimental design for a comparison of the voxel-based FE model and the PR model for (*a*) plate-rod, and (*b*) rod-rod structures. The generation of the PR model and the voxel model were illustrated only in a unit cell.

ITS-Based PR Model. The trabecular network was completely decomposed into individual plates and rods and modeled. In brief, digital topological analyses based skeletonization [23] was applied first to erode the image into a representation of the surfaces and curves skeleton while preserving the topology and morphology of the plate/rod structure. Then, a digital topological classification was performed in which each voxel on the surfaces and curves skeleton was uniquely classified as belonging to plate, rod, plate-rod junction, or rod-rod junction [24]. Based on the segmented microstructure, each square plate was modeled by multiple triangular shell elements and each rod was modeled by a two-node beam element with circular cross-section. The thickness of the shell and the diameter of the beam elements were evaluated after reconstructing the 3D volume of individual plates and rods [8].

Voxel-Based Model. A voxel-based μFE model was directly generated from each simulated μCT image by converting each voxel to an eight-node brick element [25].

μFE Analyses. Both the voxel-based and PR models were interfaced with a commercial software Abaqus (SIMULIA, Dassault Systemes, Providence, RI) to perform the μFE analyses. Given the relatively uniform yield strain of trabecular bone across anatomic sites [2,3], this study adopted a new constitutive model recently proposed by Gupta [26] in which the yield surface is generated from the principle strain space to eliminate the effect of heterogeneity in trabecular bone failure. The new constitutive law was implemented via UMAT, a material model interface in Abaqus. Trabecular bone was modeled as an isotropic linear elastic material with a Young's modulus (E_s) of 15 GPa and a Poisson's ratio of 0.3. The tissue-level yield strains are 0.33% in tension and 0.81% in compression. Approximately 5% post-yield hardening was used. For each trabecular microstructural model, a uniaxial compression test was performed to calculate the apparent Young's modulus (E^*) and apparent yield strength of trabecular bone (σ_y^*).

Statistical Analysis. The normalized Young's modulus (E^*/E_s) and yield strength (σ_y^*/E_s) predicted by the PR FE models were correlated with those of the voxel-based models by linear regression using the statistical software NCSS 2007 (NCSS LLC, Utah). Then, R^2 was calculated for each linear regression which showed the strength of the linear correlation between the two data sets.

Results

The stress-strain curves of the PR models under uniaxial compression up to 1.5% strain was highly consistent with those of voxel-based models for the plate-rod structure with elements of varying thickness and rod-rod structures with thin elements, as shown in Fig. 2. However, deviations appeared in the rod-rod structure with thick elements with trabecular thicknesses of 240 μm and 320 μm (paired t-test $p < 0.05$), which suggested the PR models to be less stiff than voxel-based models when trabecular rods are relatively thick. For both plate-rod and rod-rod structures, the normalized Young's modulus and yield strength predicted by the PR models strongly correlated with those of the voxel-based models ($R^2 \geq 0.99$) at any voxel size: 20, 40, and 80 μm (see Fig. 3). At each voxel size, the correlation was calculated between the PR and voxel-based models with four different trabecular thicknesses. Both the PR and voxel-based models for the plate-rod structure were highly robust to the resolution of images and the thickness of the trabeculae and, furthermore, provided nearly identical predictions of Young's modulus and the yield strength at any voxel size for a trabecular network of any

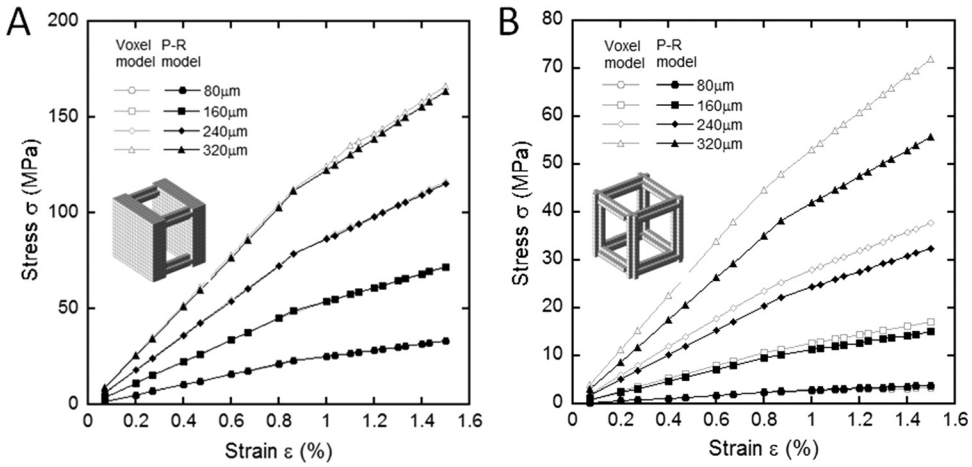

Fig. 2 Stress–strain curves under a uniaxial compression test of the idealized (*a*) plate-rod structure, and (*b*) rod-rod structure with varying trabecular thicknesses: 80, 160, 240, and 320 μm (voxel size: 20 μm)

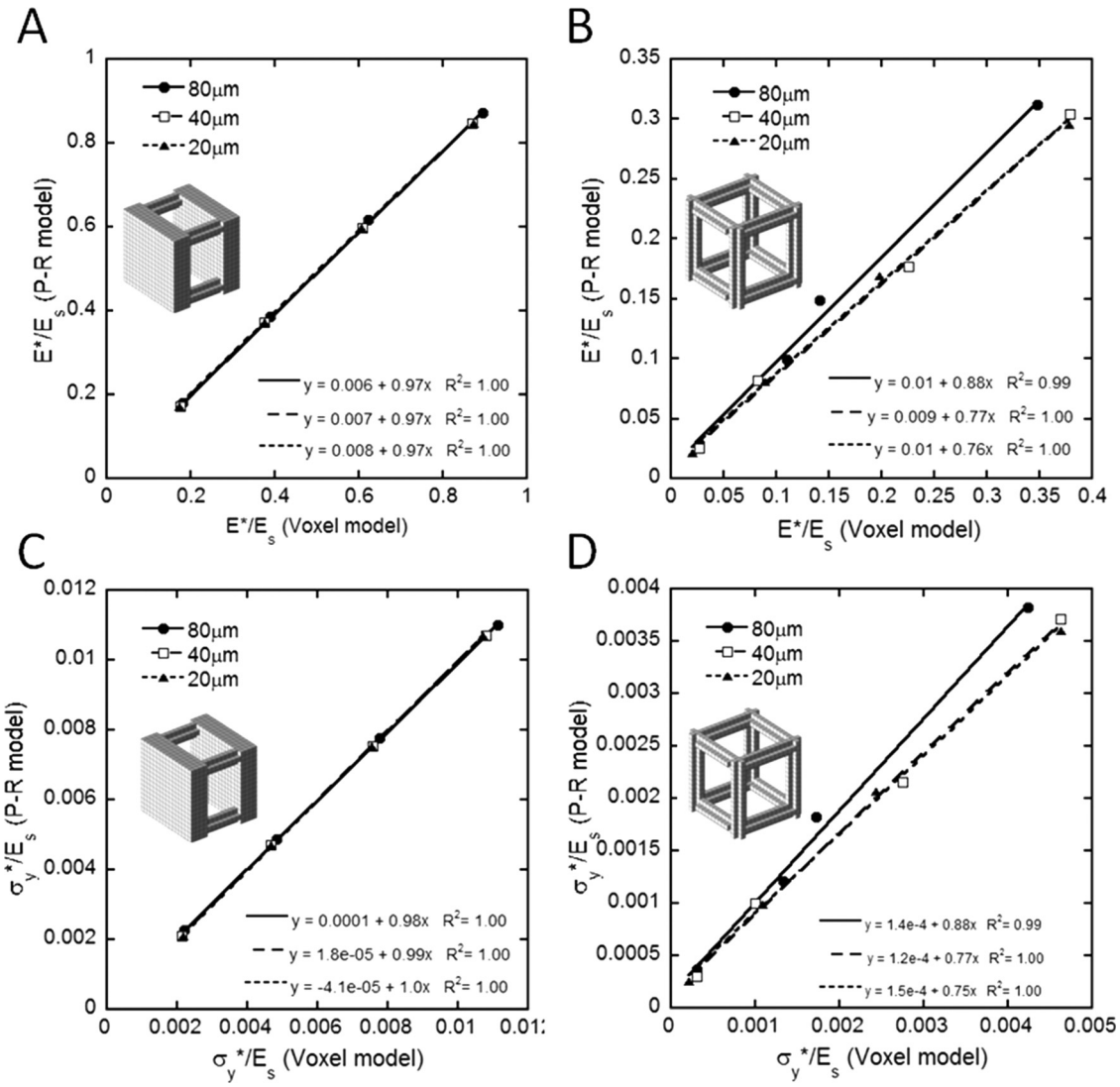

Fig. 3 Linear correlation of the normalized Young's modulus E^*/E_s between the PR and voxel models for the idealized (*a*) plate-rod structure, and (*b*) rod-rod structure; correlation of normalized yield strength σ_y^*/E_s between the PR and voxel models for the idealized (*c*) plate-rod structure, and (*d*) rod-rod structure

Table 1 Comparison of axial mechanical property of the PR model and the voxel model for the idealized plate-rod and rod-rod microstructure

		Young's modulus (GPa)					
		Voxel size					
		80 μm		40 μm		20 μm	
		Model type					
	Thickness (BV/TV)	Voxel	PR	Voxel	PR	Voxel	PR
Plate-rod trabecular microstructure	80 μm (0.16)	2.71	2.70	2.61	2.60	2.60	2.60
	160 μm (0.32)	5.84	5.78	5.63	5.58	5.63	5.58
	240 μm (0.42)	9.35	9.24	9.12	8.95	9.08	8.95
	320 μm (0.56)	13.42	13.10	13.04	12.71	13.08	12.71
		Yield strength (MPa)					
		Voxel size					
		80 μm		40 μm		20 μm	
		Model type					
	Thickness (BV/TV)	Voxel	PR	Voxel	PR	Voxel	PR
	80 μm (0.16)	33.21	34.02	32.27	31.37	32.29	31.37
	160 μm (0.32)	72.66	72.90	69.90	70.47	69.98	70.47
	240 μm (0.42)	116.49	116.64	113.36	112.99	113.00	112.99
	320 μm (0.56)	167.08	165.23	162.23	160.37	160.28	160.37
		Young's modulus (GPa)					
		Voxel size					
		80 μm		40 μm		20 μm	
		Model type					
	Thickness (BV/TV)	Voxel	PR	Voxel	PR	Voxel	PR
Rod-rod trabecular microstructure	80 μm (0.04)	0.40	0.44	0.40	0.38	0.30	0.32
	160 μm (0.15)	1.65	1.49	1.23	1.23	1.34	1.21
	240 μm (0.27)	2.12	2.24	3.38	2.65	2.97	2.54
	320 μm (0.40)	5.21	4.68	5.68	4.56	5.67	4.43
		Yield strength (MPa)					
		Voxel size					
		80 μm		40 μm		20 μm	
		Model type					
	Thickness (BV/TV)	Voxel	PR	Voxel	PR	Voxel	PR
	a80 μm (0.04)	4.57	5.44	4.68	4.58	3.08	3.89
	160 μm (0.15)	20.11	18.22	15.02	14.99	16.34	14.80
	240 μm (0.27)	25.80	27.29	41.32	32.41	36.42	31.02
	320 μm (0.40)	63.64	57.30	69.44	55.66	69.38	54.02

thickness (see Table 1). Such a consensus remained but weakened in the rod-rod structure, with the PR model predictions generally lower in magnitude than those of the voxel-based models. In addition, the PR models achieved an ~762-fold major reduction in the largest model size from ~167,680 elements in a voxel-based model to ~220 elements in a PR model, which markedly increased the computational efficiency of the μFE analysis.

Discussion

In this study, a simplified PR model of human trabecular bone was quantified in nonlinear FE analysis for the determination of the elastic and yield properties of trabecular bone. The accuracy of the PR model was examined on idealized plate-rod and rod-rod trabecular microstructures, which demonstrated its excellent predictive power with reference to corresponding voxel-based models. The wide applicability of novel PR models was evident from its superior accuracy at both μCT resolution and HR-pQCT resolution, over a broad range of trabecular thickness. Human trabecular bone is mostly either plate-predominant or a combination of plates and rods at the femur neck, proximal tibia, and vertebral body [8], where osteoporotic fractures occur most frequently. While the rod-predominant structure exists in extremely osteoporotic trabecular bone, the trabecular thickness is approximately

100 μm on average at the distal tibia and radius [27], in which case the PR model provided an accurate estimation of the Young's modulus and yield strength, similar to those for plate-rod structures. The deviation of the PR model predictions from the voxel model in the thick rod-rod structure was partly caused by the limitation of the beam theory, such as the shear deflection effects at a low beam length-to-thickness ratio [28]. Although we have examined the elastic-plastic behaviors of the trabecular bone model, this approach could be applicable to other nonlinear phenomena such as viscoelastic simulations.

Moreover, a tremendous reduction in the element number and CPU time was achieved by the conversion from voxel models to PR models. Nonlinear FE analysis for a $5.6 \times 5.6 \times 5.6$ mm^3 trabecular bone cube can be done within 14 s by a PC using the HR-pQCT-based PR model, which requires 5 h using the HR-pQCT-based voxel model and 246 h using μCT-based voxel model (unpublished work). There have been other groups trying to assess the mechanical properties of trabecular bone using beam-shell or beam FE models [9,10]. They have demonstrated the excellent predictive power of the beam-shell model in estimating the elastic modulus by linear FE analysis with an average 33-fold reduction in CPU time. Our ITS-based PR modeling technique has multiple advantages compared to their approach in terms of higher efficiency, an average 900-fold reduction in CPU time for a nonlinear FE analysis, accurate prediction of both the elastic modulus and yield strength by nonlinear FE analysis, and similarly excellent performance on clinical HR-pQCT images.

There are several limitations in this newly developed technique. First, the low resolution of the source images, e.g., an 82 μm voxel size in the HR-pQCT scans, remains a major challenge for the PR models to maintain predictive accuracy despite the loss of structural details. Second, the moduli and yield strengths predicted by the PR models were generally underestimated to some degree, which possibly resulted from the neglect of the thickening effect near trabecular joints that positively contributes to the mechanical competence of trabecular bone [29]. Lastly, given the altered details in the microstructure of trabecular bone by the PR assumption, this approach may not be applicable for microcrack development of damage accumulation.

This technical brief provides fundamental evidence for the accuracy of PR μFE models based on idealized trabecular microstructure. In future studies, the PR model will be tested on μCT and HR-pQCT images and validated against experimental measurements and gold standard μCT-based voxel μFE models. With accuracy combined with efficiency, the specimen-specific PR model shows great promise as a powerful tool for the future assessment of trabecular bone failure, damage accumulation, and fracture risks.

Acknowledgment

This work was partially supported by grants from the National Institutes of Health (Grant No. AR051376). The authors thank the support from the National Natural Science Foundation of China through Grant No. 11025208.

References

[1] NIH Consensus Development Panel on Osteoporosis Prevention, 1991, "Consensus Development Conference Report: Prophylaxis and Treatment of Osteoporosis," Osteoporosis Int., **1**(2), pp. 114–117.
[2] Liu, X. S., Sajda, P., Saha, P. K., Wehrli, F. W., and Guo, X. E., 2006, "Quantification of the Roles of Trabecular Microarchitecture and Trabecular Type in Determining the Elastic Modulus of Human Trabecular Bone," J. Bone Miner. Res., **21**(10), pp. 1608–1617.
[3] Muller, R., Hildebrand, T., Hauselmann, H. J., and Ruegsegger, P., 1996, "In Vivo Reproducibility of Three-Dimensional Structural Properties of Noninvasive Bone Biopsies Using 3D-pQCT," J. Bone Miner. Res., **11**(11), pp. 1745–1750.
[4] Chung, H. W., Wehrli, F. W., Williams, J. L., and Wehrli, S. L., 1995, "Three-Dimensional Nuclear Magnetic Resonance Microimaging of Trabecular Bone," J. Bone Miner. Res., **10**(10), pp. 1452–1461.
[5] Kinney, J. H., Lane, N. E., and Haupt, D. L., 1995, "In Vivo, Three-Dimensional Microscopy of Trabecular Bone," J. Bone Miner. Res., **10**(2), pp. 264–270.
[6] Morgan, E. F., Bayraktar, H. H., Yeh, O. C., Majumdar, S., Burghardt, A., and Keaveny, T. M., 2004, "Contribution of Inter-Site Variations in Architecture to Trabecular Bone Apparent Yield Strains," J. Biomech., **37**(9), pp. 1413–1420.
[7] Van Rietbergen, B., Odgaard, A., Kabel, J., and Huiskes, R., 1998, "Relationships Between Bone Morphology and Bone Elastic Properties Can be Accurately Quantified Using High-Resolution Computer Reconstructions," J. Orthop. Res., **16**(1), pp. 23–28.
[8] Liu, X. S., Sajda, P., Saha, P. K., Wehrli, F. W., Bevill, G., Keaveny, T. M., and Guo, X. E., 2008, "Complete Volumetric Decomposition of Individual Trabecular Plates and Rods and Its Morphological Correlations With Anisotropic Elastic Moduli in Human Trabecular Bone," J. Bone Miner. Res., **23**(2), pp. 223–235.
[9] van Lenthe, G. H., Stauber, M., and Muller, R., 2006, "Specimen-Specific Beam Models for Fast and Accurate Prediction of Human Trabecular Bone Mechanical Properties," Bone, **39**(6), pp. 1182–1189.
[10] Vanderoost, J., Jaecques, S. V., Van der Perre, G., Boonen, S., D'Hooge, J., Lauriks, W., and van Lenthe, G. H., 2011, "Fast and Accurate Specimen-Specific Simulation of Trabecular Bone Elastic Modulus Using Novel Beam-Shell Finite Element Models," J. Biomech., **44**(8), pp. 1566–1572.
[11] Liu, X. S., Bevill, G., Keaveny, T. M., Sajda, P., and Guo, X. E., 2009, "Micromechanical Analyses of Vertebral Trabecular Bone Based on Individual Trabeculae Segmentation of Plates and Rods," J. Biomech., **42**(3), pp. 249–256.
[12] Liu, X. S., Zhang, X. H., and Guo, X. E., 2009, "Contributions of Trabecular Rods of Various Orientations in Determining the Elastic Properties of Human Vertebral Trabecular Bone," Bone, **45**(2), pp. 158–163.
[13] Liu, X. S., Zhang, X. H., Sekhon, K. K., Adams, M. F., McMahon, D. J., Bilezikian, J. P., Shane, E., and Guo, X. E., 2010, "High-Resolution Peripheral Quantitative Computed Tomography Can Assess Microstructural and Mechanical Properties of Human Distal Tibial Bone," J. Bone Miner. Res., **25**(4), pp. 746–756.
[14] Liu, X. S., Shane, E., McMahon, D. J., and Guo, X. E., 2011, "Individual Trabecula Segmentation (ITS)–Based Morphological Analysis of Microscale Images of Human Tibial Trabecular Bone at Limited Spatial Resolution," J. Bone Miner. Res., **26**(9), pp. 2184–2193.
[15] Liu, X. S., Cohen, A., Shane, E., Stein, E., Rogers, H., Kokolus, S. L., Yin, P. T., McMahon, D. J., Lappe, J. M., Recker, R. R., and Guo, X. E., 2010, "Individual Trabeculae Segmentation (ITS)–Based Morphological Analysis of High-Resolution Peripheral Quantitative Computed Tomography Images Detects Abnormal Trabecular Plate and Rod Microarchitecture in Premenopausal Women With Idiopathic Osteoporosis," J. Bone Miner. Res., **25**(7), pp. 1496–1505.
[16] Liu, X. S., Stein, E. M., Zhou, B., Zhang, C. A., Nickolas, T. L., Cohen, A., Thomas, V., McMahon, D. J., Cosman, F., Nieves, J., Shane, E., and Guo, X. E., 2012, "Individual Trabecula Segmentation (ITS)-Based Morphological Analyses and Microfinite Element Analysis of HR-pQCT Images Discriminate Postmenopausal Fragility Fractures Independent of DXA Measurements," J. Bone Miner. Res., **27**(2), pp. 263–272.
[17] Beaupre, G. S., and Hayes, W. C., 1985, "Finite Element Analysis of a Three-Dimensional Open-Celled Model for Trabecular Bone," ASME J. Biomech. Eng., **107**(3), pp. 249–256.
[18] Gibson, L. J., 1985, "The Mechanical Behaviour of Cancellous Bone," J. Biomech., **18**(5), pp. 317–328.
[19] Guo, X. E., and Kim, C. H., 2002, "Mechanical Consequence of Trabecular Bone Loss and Its Treatment: A Three-Dimensional Model Simulation," Bone, **30**(2), pp. 404–411.
[20] Silva, M. J., and Gibson, L. J., 1997, "Modeling the Mechanical Behavior of Vertebral Trabecular Bone: Effects of Age-Related Changes in Microstructure," Bone, **21**(2), pp. 191–199.
[21] Yeh, O. C., and Keaveny, T. M., 2001, "Relative Roles of Microdamage and Microfracture in the Mechanical Behavior of Trabecular Bone," J. Orthop. Res., **19**(6), pp. 1001–1007.
[22] Zysset, P. K., Ominsky, M. S., and Goldstein, S. A., 1998, "A Novel 3D Microstructural Model for Trabecular Bone: I. The Relationship Between Fabric and Elasticity," Comput. Methods Biomech. Biomed. Eng., **1**(4), pp. 321–331.
[23] Saha, P. K., Chaudhuri, B. B., and Majumder, D. D., 1997, "A New Shape Preserving Parallel Thinning Algorithm for 3D Digital Images," Pattern Recogn., **30**(12), pp. 1939–1955.
[24] Saha, P. K., and Chaudhuri, B. B., 1996, "3D Digital Topology Under Binary Transformation With Applications," Comput. Vis. Image Underst., **63**(3), pp. 418–429.
[25] Hollister, S. J., 1994, "A Homogenization Sampling Procedure for Calculating Trabecular Bone Effective Stiffness and Tissue Level Stress," J. Biomech., **27**(4), pp. 433–444.
[26] Gupta, A., Bayraktar, H., Fox, J., Keaveny, T., and Papadopoulos, P., 2007, "Constitutive Modeling and Algorithmic Implementation of a Plasticity-Like Model for Trabecular Bone Structures," Comput. Mech., **40**(1), pp. 61–72.
[27] Stein, E. M., Liu, X. S., Nickolas, T. L., Cohen, A., Thomas, V., McMahon, D. J., Zhang, C., Yin, P. T., Cosman, F., Nieves, J., Guo, X. E., and Shane, E., 2010, "Abnormal Microarchitecture and Reduced Stiffness at the Radius and Tibia in Postmenopausal Women With Fractures," J. Bone Miner. Res., **25**(12), pp. 2572–2581.
[28] Ghugal, Y. M., and Sharma, R., 2011, "A Refined Shear Deformation Theory for Flexure of Thick Beams," Lat. Am. J. Solids Struct., **8**(2), pp. 183–195.
[29] Kim, H. S., and Al-Hassani, S. T., 2002, "A Morphological Model of Vertebral Trabecular Bone," J. Biomech., **35**(8), pp. 1101–1114.